Diffractive Focusing of Waves in Time and in Space

Dror Weisman,[1,*] Shenhe Fu,[1,2,3] Manuel Gonçalves,[4] Lev Shemer,[5] Jianying Zhou,[2]
Wolfgang P. Schleich,[6,7] and Ady Arie[1]

[1]*Department of Physical Electronics, Faculty of Engineering, Tel-Aviv University, Tel-Aviv 69978, Israel*
[2]*State Key Laboratory of Optoelectronic Materials and Technologies, Sun Yat-sen University, Guangzhou 510275, China*
[3]*Department of Optoelectronic Engineering, Jinan University, Guangzhou 510632, China*
[4]*Institute of Experimental Physics, Ulm University, Albert-Einstein-Allee 11, D-89081 Ulm, Germany*
[5]*School of Mechanical Engineering, Faculty of Engineering, Tel-Aviv University, Tel-Aviv 69978, Israel*
[6]*Institute of Quantum Physics and Center for Integrated Quantum Science and Technology (IQ^{ST}), Ulm University,
Albert-Einstein-Allee 11, D-89081 Ulm, Germany*
[7]*Hagler Institute for Advanced Study at Texas A&M University, Texas A&M AgriLife Research,
Institute for Quantum Science and Engineering (IQSE), and Department of Physics and Astronomy, Texas A&M University,
College Station, Texas 77843-4242, USA*
(Received 17 July 2016; published 12 April 2017)

We study the general wave phenomenon of diffractive focusing from a single slit for two types of waves and demonstrate several properties of this effect. Whereas in the first situation, the envelope of a surface gravity water wave is modulated in time by a rectangular function, leading to temporal focusing, in the second example, surface plasmon polariton waves are focused in space by a thin metal slit to a transverse width narrower than the slit itself. The observed evolution of the phase carrier of the water waves is measured for the first time and reveals a nearly flat phase as well as an 80% increase in the intensity at the focal point. We then utilize this flat phase with plasmonic beams in the spatial domain, and study the case of two successive slits, creating a tighter focusing of the waves by putting the second slit at the focal point of the first slit.

The diffraction of waves by slits has been studied for centuries [1] starting with light and culminating in matter waves of electrons [2], atoms [3], neutrons [4], and molecules [5]. According to conventional wisdom, a wave that has passed through a slit will expand. However, this popular picture is incomplete since it was predicted [6] that a rectangular one-dimensional quantum wave packet created from a plane wave by a one-dimensional slit first focuses and only then expands. This counterintuitive diffractive focusing [7] is a consequence [8] of domains in phase space where the Wigner function [9] is negative [10,11].

In the present Letter we provide the first experimental verification of this phenomenon for surface gravity water waves as well as surface plasmon polaritons. For the water waves we not only demonstrate focusing by measuring the intensity distribution [12,13] but also observe the complete phase portrait [6]. Since the phase across the focus is constant we can achieve an even stronger focusing by inserting a second slit at the focus of the first one. Indeed, with surface plasmon polariton waves we observe tighter focusing by two successive slits. In addition to the exploration of this fundamental wave phenomenon, this effect has potential applications, acting as a time lens or a spatial lens for different types of waves, in particular, in cases in which traditional lenses cannot be realized in a simple manner.

We start by studying the phenomenon of temporal diffractive focusing of surface gravity water waves generated by a wave maker in a water tank. Surface gravity water waves, matter waves, and electromagnetic waves share similar dynamics [14–16]. Specifically, for water waves with low steepness, the wave equation has a form similar to the Schrödinger equation of a free particle and to the paraxial Helmholtz equation [17–19]. The spatial version of this linearized wave equation in its normalized form reads [19]

$$\frac{\partial^2 A}{\partial \tau^2} - i \frac{\partial A}{\partial \xi} = 0, \tag{1}$$

where A, ξ, and τ are the amplitude envelope, the propagation coordinate, and the elapsed time, respectively. These scaled dimensionless variables are related to the ones in physical units according to $A \equiv a/a_0$, $\xi \equiv \varepsilon^2 k_0 x$, and $\tau \equiv \varepsilon \omega_0(x/c_g - t)$, where a_0 is the maximum amplitude of the envelope, $k_0 \equiv 2\pi/\lambda_0$ denotes the water wave number with the carrier wavelength λ_0, and $\varepsilon = k_0 a_0$ denotes the characteristic wave steepness. The carrier angular frequency ω_0 satisfies the deep-water dispersion relation [19] $\omega_0^2 = g k_0$, with g being the gravitational acceleration. Accordingly, the linear group velocity can be expressed as $c_g \equiv d\omega/dk = \omega_0/(2k_0)$.

The temporal rectangular water wave packet of width t_0 at the wave maker has the form

$$A(x = 0, t) \equiv \begin{cases} 1, & |t| \leq t_0/2 \\ 0, & \text{o.w.} \end{cases} \qquad (2)$$

and the evolution along the water tank is described by

$$A(\xi, \tau) = \frac{1}{2\sqrt{\pi\xi}} \exp\left(\frac{i\pi}{4}\right) \int_{-\tau_0/2}^{+\tau_0/2} \exp\left(-\frac{i}{4\xi}(\tau - \tau')^2\right) d\tau',$$
$$(3)$$

where $\tau_0 \equiv \varepsilon\omega_0 t_0$ is a dimensionless constant that is proportional to the width of the initial rectangular wave function. Hence, the temporal surface elevation including the carrier wave reads $\eta(x, t) \equiv a_0\text{Re}\{A(x, t)\exp[i(\omega_0 t - k_0 x)]\}$.

The expression in Eq. (3) is similar to the time evolution of an initial rectangular wave packet described by the Schrödinger equation of a free particle. Hence the diffractive focusing effect can be explained using Cornu spirals [6]. In Sec. (a) of Supplemental Material[20] we present an alternative explanation based on the corresponding Green function: At short distances x, the contribution from different points of the input pulse may be out of phase, leading to destructive interference, but for larger distances all contributions are in phase, but with amplitude that scales as $1/\sqrt{x}$.

Similar to the derivation made by Ref. [6], we can use the properties of the Fresnel diffraction integral and determine the spatial and temporal locations

$$\xi = \frac{1}{3\pi + 8\pi n}\left(\frac{\tau_0}{2} \pm \tau\right)^2, \quad n = 0, 1, 2... \qquad (4)$$

of the intensity extrema in the evolution of the wave packets. The maximum intensity of the wave packets is located at $\xi_f(n = 0, \tau = 0) = \tau_0^2/12\pi$ where the maximum intensity is 1.8 times larger than the incident intensity $|a_0|^2$, as suggested by Ref. [6]. This fact implies that the initially rectangular wave packet significantly shrinks during the evolution along the propagation distance and we denote $x_f = \omega_0^2 t_0^2/12 k_0 \pi$ as the focal length.

Our water wave experiments relied on a wave tank [21] shown in Fig. 1(a). In our experiments, the wavelength was selected to be $\lambda_0 = 0.76$ m, so that the dimensionless depth $k_0 h = 4.96 > \pi$ satisfied the deep-water condition. The corresponding group velocity is $c_g = 0.54$ m/s and the wave dissipation can be neglected [22]. We program the wave maker to provide a rectangular pulse with a width $t_0 = 4.18$ s, thus containing six cycles. We set $a_0 = 6$ mm ($\varepsilon = 0.05$); hence, the induced nonlinearity could be neglected.

We have also experimentally examined the phase evolution of such rectangular wave packets along the tank. The envelope phase $\psi_2(t)$ can be determined by the phase
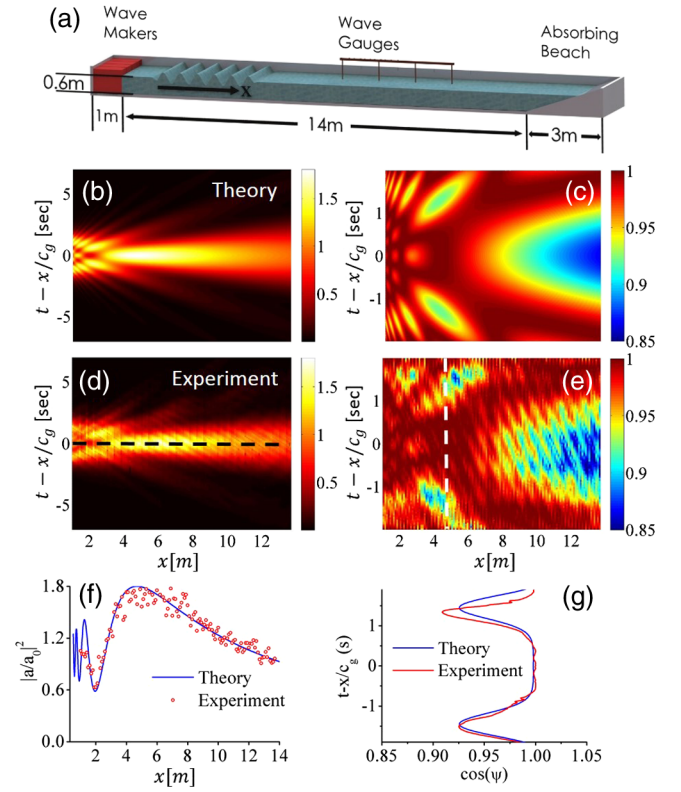
FIG. 1. Theoretical prediction and experimental observation of diffractive focusing of water wave packets with width $t_0 = 4.18$ s corresponding to six cycles. A schematic illustration is given of the experimental setup (a), theoretical and experimental results representing the intensity evolution $|a|^2/|a_0|^2$ of the wave packets along the tank [(b) and (d)], and of the envelope phase evolution [(c) and (e)] given by $\cos\psi$. Panels (f) and (g) display the spatial and temporal evolution of intensity and phase along the dashed lines in (d) and (e), respectively.

difference between two elevations at different locations of the tank. According to Ref. [23], it can be expressed as

$$\psi_2(t) = [\psi_{A_2}(t) + k_0 x_2] - [\psi_{A_1}(t) + k_0 x_1] - \psi_1(t), \qquad (5)$$

where ψ_{A_j} with $j = 1, 2$ represents the phase of the envelope after Hilbert transforming the wave elevations at two different locations x_1, x_2. More details about the calculation can be found in Supplemental Material of Ref. [23]. According to Eq. (2), we note that $\psi_1(t, x_1 = 0) = 0$. In order to avoid the 2π-phase ambiguity, the envelope phase evolution of such rectangular wave packets was illustrated as a cosine function of time, i.e., $\cos\psi$.

Figure 1 presents theoretical and experimental results confirming the phenomenon of diffractive focusing for the example of the generated rectangular wave packets. The recorded elevations were presented in a system traveling at the linear group velocity c_g. The experimental results match well the theory based on Eq. (3), exhibiting clearly the focusing effect with a focal point at $x = 4.6$ m. It is worth

noting that the calculated and observed intensity patterns from Figs. 1(b) and 1(f) are similar to those observed by Vitrant *et al.* [12] for the case of light beams diffracting from a slit. To further highlight the temporal focusing of the wave, we present intensity profile slices as a function of time along the propagation axis in Sec. (b) of Supplemental Material[20].

Close to the focal region the phase becomes nearly invariant with time as shown in Fig. 1(g). This observation is the first experimental confirmation of the prediction [6] of a constant phase near the focal region. One can now place another slit at the focal point and further focus the pulse, since the phase distribution is similar to that at the origin. We demonstrate this possibility below in the spatial domain using surface plasmon polariton waves.

The phenomenon of diffractive focusing is further confirmed by quantitatively observing the pronounced decrease of the pulse width. However, an appropriate measure for the pulse width is required, since the naive criterion of the second moment of a real and symmetric initial wave function always increases during its evolution [24], because the second moment gives a large weight to values far from the axis. The influence of the tails of the pulse can be reduced by applying a Gaussian window [6],

$$W(\kappa, x) \equiv \frac{1}{\kappa^2} \left[1 - \frac{\int_{-\infty}^{\infty} |\eta(t,x)|^2 e^{-(\kappa t)^2} dt}{\int_{-\infty}^{\infty} |\eta(t,x)|^2 dt} \right], \quad (6)$$

leading us to the normalized width $\delta W(\kappa, x) \equiv W(\kappa, x)/W(\kappa, 0)$. Here κ is a parameter with dimensions that are inverse to the size of the slit. Our measurements displayed in Fig. 2(a) reveal the contraction of the pulse and match well the theory.

Moreover, we have measured the location x_f of the maximum intensity for rectangular wave packets with different widths t_0, as shown in Fig. 2(b). Clearly, the experimental results correspond to the theory, demonstrating that the focal length x_f increases quadratically with t_0.

So far we have investigated the temporal focusing of rectangular water wave packets. Next we demonstrate the analogous wave phenomenon in space using surface plasmon polariton (SPP) waves. These are surface
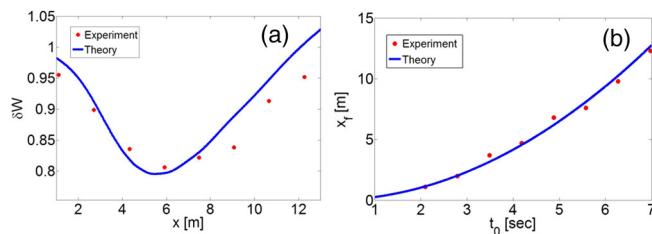
FIG. 2. Theoretical predictions (solid line) and experimental results (dots) of the normalized Gaussian temporal width δW with a value of $\kappa t_0 = 4.7$ for a slit with a width of $t_0 = 4.18$ s (a), and the focal length, x_f, in its dependence on the pulse width t_0 (b).

electromagnetic waves that are coupled to collective charge oscillations that propagate at the interface between a dielectric and a metallic medium. The ability to focus SPP waves was demonstrated by several other methods, including nanometric slits, holes, and loadings on circular and elliptical structures [25–28], and also by using an in-plane Fresnel zone plate [29]. However, so far a simple slit has not been employed as a focusing element for these waves.

In the paraxial approximation, the two-dimensional Helmholtz equation for the SPP envelope [30] reads

$$\frac{\partial^2 A}{\partial y^2} + 2i k_{SP} \frac{\partial A}{\partial z} = 0, \quad (7)$$

where $k_{SP} \equiv k_0 \sqrt{\varepsilon_m \varepsilon_d / (\varepsilon_m + \varepsilon_d)}$ and k_0 denotes the free-space wave vector. The permittivity of the metal and the dielectric are ε_m and ε_d, respectively.

We emphasize that Eq. (7) is of the form of the Schrödinger equation for a free particle. Hence, a SPP wave can also be focused [6] by a single slit, but in space rather than in time. In the case of plasmonic waves, y and z are the transverse and propagation variables, replacing t and x in water waves, respectively.

Since SPPs can only propagate at the interface between a metal and a dielectric, we chose to fabricate [31] a "plasmonic slit" by removing metal regions, thereby keeping only a narrow metallic area, which connects the two wide metallic surfaces depicted in Figs. 3(a) and 3(b). In this way, the SPP is forced to propagate through the narrow aperture defined by the metal region. We have used *e*-beam lithography followed by evaporation of silver to fabricate a silver grating with a period of 1.055 μm, enabling excitation with a free space beam at normal incidence [32].

As apparent from Fig. 3, the slit has a relatively large length of 10 μm. This value was chosen in order to eliminate the unwanted effect of tunneling of the wave through the metal gap, which becomes significant when the gap length is only a few microns. We have noticed that for a shorter gap of only 4 μm, a significant part of the plasmonic wave energy still propagates due to tunneling.

To simulate the intensity distribution of the plasmonic plane wave that is propagating through the slit, we have realized a numerical code based on the two-dimensional Green function [30] of the Helmholtz equation. We have used the values [33] $\varepsilon_m = -58.04 + i0.61$ and $\varepsilon_d = 1$ for the silver and air permittivity, respectively.

The plasmonic beam was generated by illuminating a silver grating and its distribution was measured using a NSOM [34]. Figure 3 shows the results for two different slits. Indeed, Figs. 3(a)–3(d) present scanning electron microscope and NSOM measurements, topography of the sample, and intensity distribution of a plasmonic plane wave that propagates through a 14 μm wide and 10 μm long single slit. Figures 3(e) and 3(f) show the numerical
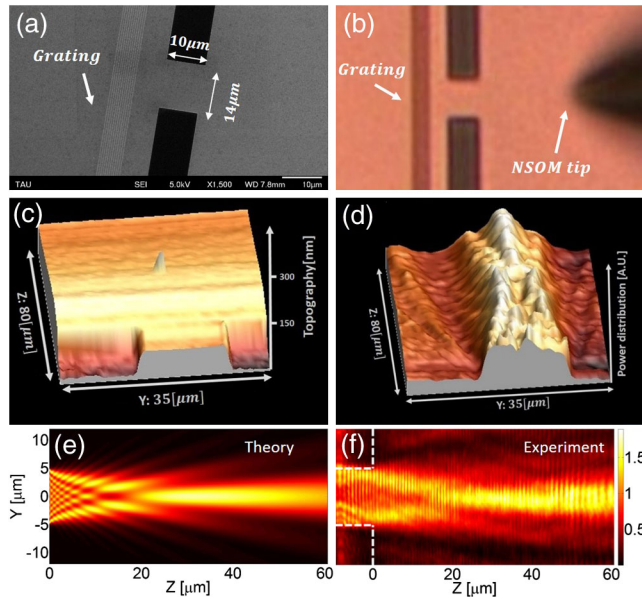
FIG. 3. Diffractive focusing of a plasmonic wave from a $14 \times 10\ \mu m$ slit: scanning electron microscope image of the sample (a) and a picture taken by the near-field scanning optical microscope (NSOM) camera (b); three-dimensional representation of the NSOM measurements of the topography of the sample (c), and of the intensity distribution of the SPP (d); numerical simulation (e) of diffractive focusing for another slit with dimensions $10 \times 10\ \mu m$; and the NSOM measurement of the corresponding SPP intensity distribution (f). The white dashed line in (f) represents the slit topography.

simulations and the NSOM intensity measurements of a slit with a width of $10\ \mu m$. The effect of the focusing is clearly visible. We note that the maximum intensity in the focal plane is less than 1.8 times the incident intensity (as measured for the case of light beams [8,12]) due to plasmonic losses.

After having observed that a single slit can focus a plasmonic wave, we are able to enhance the focusing effect, by adding a second slit after the first as shown in Fig. 4(a). We chose the second slit to be at the focus of the first slit as determined by our simulations. This time, the wave that propagates through the second slit does not have a perfectly flat phase and intensity distributions, but ones derived from the propagation through the first slit. However, as predicted in Ref. [6] and confirmed by our water wave experiment above, the phase profile at the focal plane is almost constant.

Figure 4(a) shows the microscope picture of our structure with two slits, the first $14\ \mu m$ wide and $10\ \mu m$ long, and the second $5\ \mu m$ wide and $4\ \mu m$ long. Moreover, Figs. 4(b) and 4(c) present the numerical simulations and the corresponding NSOM intensity measurements of the two-slits structure, respectively. The plasmonic intensity on the edges of the metal was negligible; hence, edge reflections can be neglected. Because of limitations of the system, the measurement in Fig. 4(c) is a combination of two separate ones that overlap, and are connected at the location of the second slit.
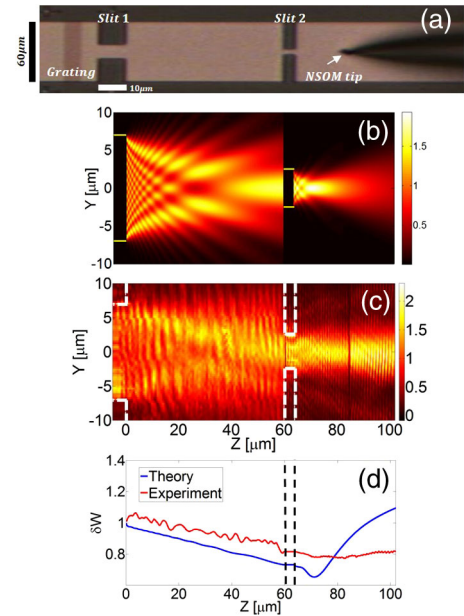
FIG. 4. Diffractive focusing of a plasmonic wave from two successive slits: the dimensions of the first slit are $14 \times 10\ \mu m$, and of the second $5 \times 4\ \mu m$. Picture of the sample taken by the NSOM camera (a), and the simulation result (b) under the assumption of an infinitesimal narrow slit. The NSOM measurement of the SPP intensity distribution (c) combines two separate images that are connected at the location of the second slit. The white dashed line represents the slit topography. Theoretical and experimental results (d) of the normalized Gaussian spatial width δW with a value of $\kappa a_1 = 3.15$ for the area after the first slit ($a_1 = 14\ \mu m$), and a value of $\kappa a_2 = 4.89$ for the domain after the second slit ($a_2 = 5\ \mu m$). The black dashed lines in (d) represent the location of the second slit. The experimental results were calculated for a reduced area given approximately by the slit size.

Figure 4(d) presents the normalized Gaussian width δW, calculated according to Eq. (6) with the following substitutions: (i) the SPP amplitude envelope A replaces the water wave amplitude η, and (ii) the integration is performed over the transverse spatial coordinate. For the two studied regions, between the first and second slit, and after the second slit, we have used two different values for the exponential decay parameter κ. For continuity, we define the value of δW after the second slit to be equal to its value just before the second slit.

After the second slit our plasmonic wave keeps its profile along tens of microns and has a relatively fixed narrow width, determined by the size of the second slit. This long-range fixed profile can be used for future plasmonic applications that require tight beams, e.g., particle manipulation along a surface [35].

The simulation in Fig. 4(b) assumes an infinitesimal thin slit for the second slit, whereas in the experiment the second slit has a length of $4\ \mu m$. In addition, the NSOM also measures some scattered light of the free-space illumination beam. These two effects may account for the difference between the calculation and the measurements in Fig. 4(d).

In summary, we have shown that water waves as well as plasmonic waves experience the effect of diffractive focusing by a temporal or a spatial slit. The ability to focus a plasmonic wave with a flat transverse phase can be used for future plasmonic applications, offering a valuable alternative to dielectric loaded plasmonic lenses [25–28]. The plasmonic slit can also be used, beyond focusing, for simple imaging tasks, as examplified in Sec. (c) of Supplemental Material[20]. Moreover, an even tighter focusing was reached by the use of two successive slits. We have also demonstrated that the size of the slit determines the location of the focus, and that in this region the phase of the wave is nearly constant, in complete agreement with the prediction of Ref. [6].

The effect of diffractive focusing can be utilized for other waves that satisfy a Schrödinger-like wave equation, including for example acoustic waves and various matter waves [5]. Furthermore, this concept can also be applied to ultrashort optical pulses. We envision focusing them in time by shaping the temporal wave packet similarly to the method applied in our water waves experiment, and/or passing them through a spatial slit and thereby focusing them in space.

---

[*]drorwei1@mail.tau.ac.il

[1] F. M. G. Grimaldi, *Physico Mathesis de Lumine, Coloribus, et Iride, Aliisque Annexis Libri Duo* (Vittorio Bonati, Bologna, Italy, 1665).

[2] C. Jönsson, Am. J. Phys. **42**, 4 (1974).

[3] J. A. Leavitt, Am. J. Phys. **37**, 905 (1969).

[4] A. Zeilinger, R. Gähler, C. G. Shull, W. Treimer, and W. Mampe, Rev. Mod. Phys. **60**, 1067 (1988).

[5] M. Arndt, O. Nairz, J. Vos-Andreae, C. Keller, G. van der Zouw, and A. Zeilinger, Nature (London) **401**, 680 (1999).

[6] W. B. Case, E. Sadurni, and W. P. Schleich, Opt. Express **20**, 27253 (2012).

[7] For a different mechanism of focusing due to chirping a super-Gaussian light pulse analyzed in the content of fiber optics, see for example G. P. Agrawal, *Nonlinear Fiber Optics* (Academic Press, New York, 2001).

[8] M. R. Gonçalves, W. B Case, A. Arie, and W. P. Schleich, Appl. Phys. B **123**, 121 (2017).

[9] W. P. Schleich, *Quantum Optics in Phase Space* (Wiley-VCH, Weinheim, 2001).

[10] I. Bialynicki-Birula, M. A. Cirone, J. P. Dahl, M. Fedorov, and W. P. Schleich, Phys. Rev. Lett. **89**, 060404 (2002).

[11] We emphasize that this phenomenon also depends strongly on the number of dimensions in which the wave propagates and is intimately related to the violation of Huygens principle in even dimensions as discussed for example by M. A. Cirone, J. P. Dahl. M. Fedorov, D. M. Greenberger, and W. P. Schleich, J. Phys. B **35**, 191 (2002).

[12] G. Vitrant, S. Zaiba, B. Y. Vineeth, T. Kouriba, O. Ziane, O. Stéphan, J. Bosson, and P. L. Baldeck, Opt. Express **20**, 26542 (2012).

[13] The innovative study of the effect reported in Ref. [12] concentrates on light and measures solely the corresponding intensity distribution in the near field of the slit.

[14] S. Fu, Y. Tsur, J. Zhou, L. Shemer, and A. Arie, Phys. Rev. Lett. **115**, 034501 (2015).

[15] A. Chabchoub, B. Kibler, C. Finot, G. Millot, M. Onorato, J. Dudley, and A. Babanin, Ann. Phys. (Berlin) **361**, 490 (2015).

[16] J. M. Dudley, F. Dias, M. Erkintalo, and G. Genty, Nat. Photonics **8**, 755 (2014).

[17] E. Lo and C. C. Mei, J. Fluid Mech. **150**, 395 (1985).

[18] E. Kit and L. Shemer, J. Fluid Mech. **450**, 201 (2002).

[19] L. Shemer and B. Dorfman, Nonlinear Processes Geophys. **15**, 931 (2008).

[20] See Supplemental Material at http://link.aps.org/supplemental/10.1103/PhysRevLett.118.154301 for (a) Physical explanation of the diffractive focusing phenomenon, (b) Intensity profiles along propagation axis, and (c) "Imaging" using a single slit.

[21] The water wave experiments were performed in an 18 m long, $l = 2$ m wide, and $h = 0.6$ m deep laboratory wave tank. Waves are excited by a computer-controlled paddle-type wave maker placed at one end of the water tank. A 3 m long wave energy absorbing beach is placed at the other end. To eliminate the effect of the beach, measurements were limited to distances not exceeding 14 m from the wave maker. The instantaneous water surface elevation at any fixed location along the tank is measured by four wave gauges mounted on a bar that is parallel to the tank side walls with a sampling frequency of 400 Hz. The bar with the gauges is fixed to an instrument carriage that can be shifted along the tank and is controlled by the computer.

[22] L. Shemer, K. Goulitski, and E. Kit, Eur. J. Mech. B **26**, 193 (2007).

[23] S. Fu, Y. Tsur, J. Zhou, L. Shemer, and A. Arie, Phys. Rev. Lett. **115**, 254501 (2015).

[24] K. Vogel, F. Gleisberg, N. Harshman, P. Kazemi, R. Mack, L. Plimak, and W. P. Schleich, Chem. Phys. **375**, 133 (2010).

[25] L. Yin, V. K. Vlasko-Vlasov, J. Pearson, J. M. Hiller, J. Hua, U. Welp, D. E. Brown, and C. W. Kimball, Nano Lett. **5**, 1399 (2005).

[26] Z. Liu, J. M. Steele, W. Srituravanich, Y. Pikus, C. Sun, and X. Zhang, Nano Lett. **5**, 1726 (2005).

[27] I. P. Radko, S. I. Bozhevolnyi, A. B. Evlyukhin, and A. Boltasseva, Opt. Express **15**, 6576 (2007).

[28] A. B. Evlyukhin, S. I. Bozhevolnyi, A. L. Stepanov, R. Kiyan, C. Reinhardt, S. Passinger, and B. N. Chichkov, Opt. Express **15**, 16667 (2007).

[29] L. Feng, K. A. Tetz, B. Slutsky, V. Lomakin, and Y. Fainman, Appl. Phys. Lett. **91**, 081101 (2007).

[30] I. Epstein, Y. Tsur, and A. Arie, Laser Photonics Rev. **10**, 360 (2016).

[31] A silicon substrate was spin coated with a polymethyl metacrylate (PMMA) resist thin film, followed by the patterning with an electron beam and development of the exposed PMMA. Then, a 150 nm silver layer was evaporated and the remaining PMMA removed by lift-off. In order to add a silver grating layer above the first one another electron beam lithography process was applied, including a spin coat of PMMA, a grating pattern, and development of the PMMA, followed by another evaporation of 50 nm of silver.

[32] S. A. Maier, *Plasmonics: Fundamentals and Applications* (Springer, New York, 2007).

[33] P. B. Johnson and R. W. Christy, Phys. Rev. B **6**, 4370 (1972).

[34] In our experiment we used a fiber-coupled diode laser emitting light with a wavelength 1064 nm. The light beam passed through a beam expander and a cylindrical lens, and was focused on the silver grating layer by a microscope objective lens. A Nanonics MultiView2000 NSOM system with a 300 nm tip was used to measure the plasmonic intensity distribution and the topography of the sample.

[35] X. Ding, S.-C. S. Lin, B. Kiraly, H. Yue, S. Li, I.-K. Chiang, J. Shi, S. J. Benkovic, and T. J. Huang, Proc. Natl. Acad. Sci. U.S.A. **109**, 11105 (2012).